International Journal of Engineering Trends and Technology
ISSN: 2231–5381 / https://doi.org/10.14445/22315381/IJETT-V74I2P125

Volume 74 Issue 2, 336-344, February 2026

Review Article

Review of the Spray Pyrolysis Technique of Thin Film

Ho Soonmin[1], K. Arjunan[2], S. Bharathkumar[3], Héctor Valdés[4]

[1]*Faculty of Health and Life Sciences, INTI International University, Putra Nilai, Negeri Sembilan, MALAYSIA.*
[2]*School of Physics, Bharathidasan University, Trichy, Tamil Nadu, India.*
[3,4]*Clean Technology Laboratory, Facultad de Ingeniería, Universidad Catolica de la Santísima Concepcion, Concepcion, Chile.*

[1]*Corresponding Author : soonmin.ho@newinti.edu.my*

Received: 28 August 2024 Revised: 07 November 2024 Accepted: 28 January 2025 Published: 14 February 2026

Abstract - *Spray pyrolysis is becoming more popular because of its affordability, convenience of use, consistency, and variety of substrate options. Photovoltaics, solar window coating, and optical imaging are among the uses for thin films made with this method. The prepared films' properties were examined through a variety of methods to study the properties of the samples. The morphologies and characteristics of the resulting films are significantly impacted by changes in the growing circumstances. The effectiveness of a material in solar cells can be significantly impacted by its shape, according to experimental results. Photon-to-electron conversion is influenced by the shape of the active layer.*

Keywords - *Thin Films, Spray Pyrolysis, Photovoltaic, Deposition, photovoltaic, Energy Efficiency, Energy Consumption.*

1. Introduction

Thin films have been prepared using many deposition techniques. In general, the deposition method [1] could be grouped into physical methods and chemical techniques. The selection of deposition method is strongly dependent on some factors such as production cost, quality of films, and applications of products [2]. The spray pyrolysis method is an affordable, non-vacuum method for producing materials such as powders and films. The pros and cons of this method have been emphasized (Table 1). One of the disadvantages was that impurity could be found in spray-deposited films. This problem could be solved using the thermal evaporation method. In the context of films [3], they are often applied to a diverse range of substrates that can be readily modified for extensive area deposition and manufacturing processes. The Spray Pyrolysis method consists of three key stages: Precursor Solution Formulation [4], Aerosol Creation and Movement, and Synthesis Process. In the initial phase, the precursor solution's chemical composition must include a compound that will produce the necessary chemical composition after the Pyrolysis Process [5]. In the second stage, the size distribution of Aerosol Droplets [6], influenced by the Aerosol Generation Method, will define the Morphological features of the final material and establish the appropriate range of synthesis temperatures [7]. In the final stage, the choice of whether the ultimate chemical reaction occurs in the gas phase or on a heated substrate will decide if the resulting material is a powder or film coating [8, 9]. The Pyrolysis Spray setup includes an atomizer [10], chemical solution, heater, and temperature regulator [11]. The atomizer is utilized to create a stream of liquid that needs to be applied to the substrate. The droplet size of the precursor solution is influenced by the atomization technique used [12]. Aerosol Spraying generates larger droplets, whereas ultrasonic spraying creates smaller droplets. The substrate is warmed on the hot plate for the coating. The two key factors influencing film thickness and surface morphology [13] are the deposition temperature and droplet size. In this work, the main objective is to prepare samples through the Spray Pyrolysis method. In general, Table 1 highlights the advantages of this deposition method. The ability to readily modify the Spray Pyrolysis method to produce large-area thin films is another advantage. The obtained films were studied using a lot of techniques such as TEM, AFM, SEM, XPS, Raman Spectroscopy, Photoluminescence Spectroscopy, EDX, and AFM.

Table 1. Advantages and disadvantages of different types of deposition techniques

Deposition method	Advantages	Disadvantages
spray pyrolysis technique	• Simple • Low-cost Reproducible • Scalable	Formation of undesirable properties could be detected at higher temperatures [14] Optimization experiments must be conducted to get the desired samples.

		Inconsistent particle size distribution could be observed [15] Low yield could be observed. Impurities could be found.
Chemical bath deposition	• Simple • Inexpensive	• Generate waste solvent • Involve hazardous chemicals
Thermal evaporation	• Can control film thickness • Require less equipment.	• Low melting point precursors • Resulted in thermal decomposition
Sputtering method	• High purity • Can control film thickness	• Low deposition rate • Equipment very costly

2. Experimental

There are several keywords, including Spray Pyrolysis, Solar Cells, Thin Film Materials, Band Gap Energy, Absorption Coefficient, and Power Conversion Efficiencies, that were searched through major databases such as Scopus, MDPI, Google Scholar, Web of Science, ACS, and Taylor & Francis. A literature survey has been carried out, and articles published from 1996 to 2024 were studied.

3. Literature Survey

The sequential ionic layer adsorption and reaction approach is a straightforward, less costly, and faster way to deposit binary semiconducting thin films. It may also be used for large-area thin-film deposition, such as that of compounds II–VI. The SILAR approach involves immersing the substrate separately into two precursor solutions, followed by a water wash to remove any loosely bound species [16]. Adsorption of the cation precursor, water washing, adsorption of the anion precursor, reaction, and further rinsing comprise one SILAR cycle. Depending on the experimental circumstances, the growth rates of thin films in the SILAR technique have ranged from a quarter to a half of a monolayer [17]. This demonstrates that during adsorption, aqua ligands remain largely intact, reducing the density of cations and anions in a single layer. On the other hand, one SILAR cycle may precisely regulate the thin film's growth.

One popular chemical method for creating supercapacitor electrodes is dip-coating. The simplicity of use, repeatability [18], and scalability of dip-coating over other production processes make it a potential method for mass-producing supercapacitor electrodes. The use of modified substrates using nanomaterials as supercapacitor electrodes has gained a lot of attention in recent years. Applying dip-coating to deposit these nanoparticles on the substrate surface improves the capacitance, cycle stability, and charge-discharge performance. The technique of dip-coating, which deposits nanomaterials on surfaces [19], is widely used to create supercapacitor electrodes.

The sol-gel process is a technique used in material science, engineering, and technology that turns tiny molecules into solid materials [20]. Metal oxides are produced using this process. During the process, monomers in solution are transformed into a colloidal solution, which serves as a precursor for an integrated network made up of either Network Polymer or Discrete Particles [21]. Ceramic particles are also produced via the sol-gel technique.

In the chemical bath deposition process, specific substrates will be cleaned and immersed in chemical solutions to form a thin layer on the substrate [22]. Numerous oxide materials, both single and multi-component, have been deposited as films at temperatures below 100 °C on substrates with vastly differing chemistries and topographies, mostly from aqueous precursor solutions. It is a thin-film deposition technique that uses an aqueous precursor solution. Heterogeneous nucleation [23] is commonly used in chemical bath deposition to create homogeneous thin coatings of metal chalcogenides. It was noted that chemical bath deposition is considered a low-cost film production method that yields consistent results with minimal infrastructure.

Like Electrophoretic Deposition, Electrochemical deposition also happens in an Electrochemical Cell [24]; however, unlike Electrophoretic Deposition, a chemical bonding process takes place in this instance. The Magnesium substrate acts as one of the electrodes in an Electrochemical Cell that is filled with a monomer solution for Electrochemical deposition [25]. The monomers chemically polymerise onto the magnesium when voltage is supplied.

X-ray Photoelectron Spectroscopy (XPS) was used to examine the surface chemical composition (Figure 1). It was noticed that several peaks, such as Mn (2p3/2), (2p1/2), and O (1s), indicated the presence of Mn_3O_4 phases in Magnesium-Doped Manganese Oxide compounds. Binding energies were found to be 640.4 eV and 641-641.5 eV, representing pure and doped samples, respectively. This is in line with pure films showing the MnO compound growing, whereas Mg-doped films display the Mn_3O_4 development. Figure 1 indicates XPS spectra of Mn (2p) core levels; the 2p3/2 peak is really made up of two components [26]: one component is located at 641.5 eV (Table 1), and the other at 639.5 eV. This highlights the formation of two MnO and Mn_3O_4 molecules and validates the occurrence of two distinct valences, $Mn2^+$ and

$Mn3^{+}$. Tetragonal phase, and nanograins were mentioned in XRD and SEM studies, respectively. The surface of the manganese oxide sheets is porous, rough, and textured as seen by AFM. The larger size of the $Mg2^{+}$ ion in the manganese oxide lattice is thought to have an impact on the band gap's reduction.

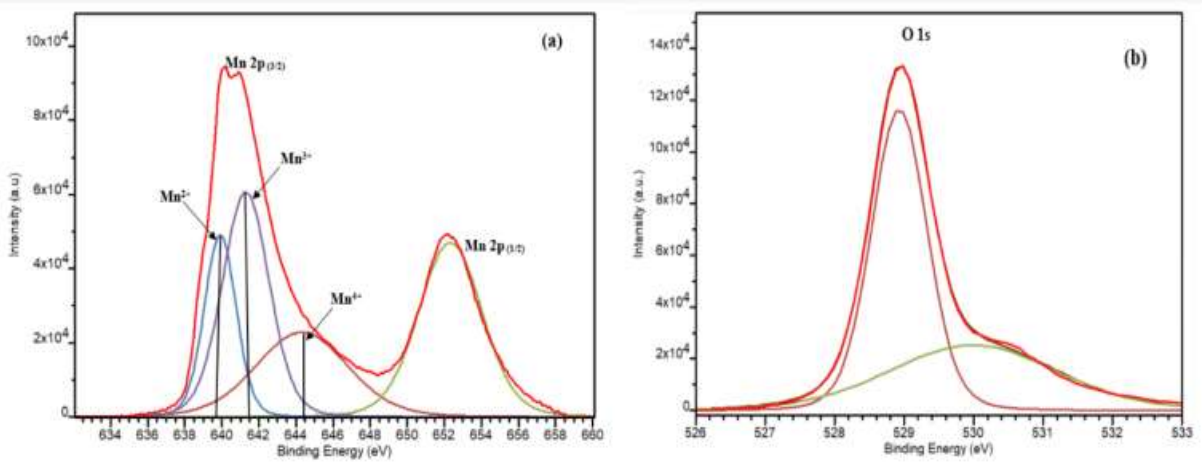

Fig. 1 XPS studies of oxygen and manganese elements (a) Mn (2p3/2) and Mn (2p1/2) peaks, and (b) O (1s) core level [26].

Extensive research has been conducted on the use of Tungsten Oxide (WO_3) in gas sensors, displays, Electrochromic Windows, and Switchable Mirrors. It is non-toxic with a band gap of 2.6-3 eV. This material could be used for Electrochromic applications due to its advantageous coloration efficiency and excellent fast response time. Results show that broad grain boundaries or high porosity improved coloration efficiency and speed up switching between the colored and bleached phases. The results of these Chronoamperometry tests showed that the color and bleaching of the films had separate temporal responses of 9 and 4 seconds, respectively. Because of the way the films grow and form on the substrate, samples formed with 0.1 M solution exhibit an increase in charge density. In addition, it was found that the films produced from a lower precursor concentration develop more slowly than other samples. Regarding precursor concentration and volume variations, there are only minor, non-trending variations in the range of time constant values. SEM characterization reveals a unique micro-structured morphology of the WO_3 thin films. The microstructures consist of a Polycrystalline WO_3 Granular Nanocrystalline background with randomly distributed bubble-like islands and wall-like features. The films' surface morphology and structure mainly remained unchanged with respect to thickness and concentration, exhibiting only slight variations in terms of size and feature density. These first SEM findings imply that thicker films with lower precursor concentrations have more compact features. It seems that films with less compact form and lower thickness are more favorable for the Electrochromic process. In terms of Raman studies (Figure 2), the Monoclinic Phase of WO_3 could be identified through several peaks such as 269, 711, and 803 cm^{-1}. Peaks connected to the ε phase are present at wavenumbers 326, 421, and 679. The lattice vibration is represented by a band at 120 cm^{-1}.

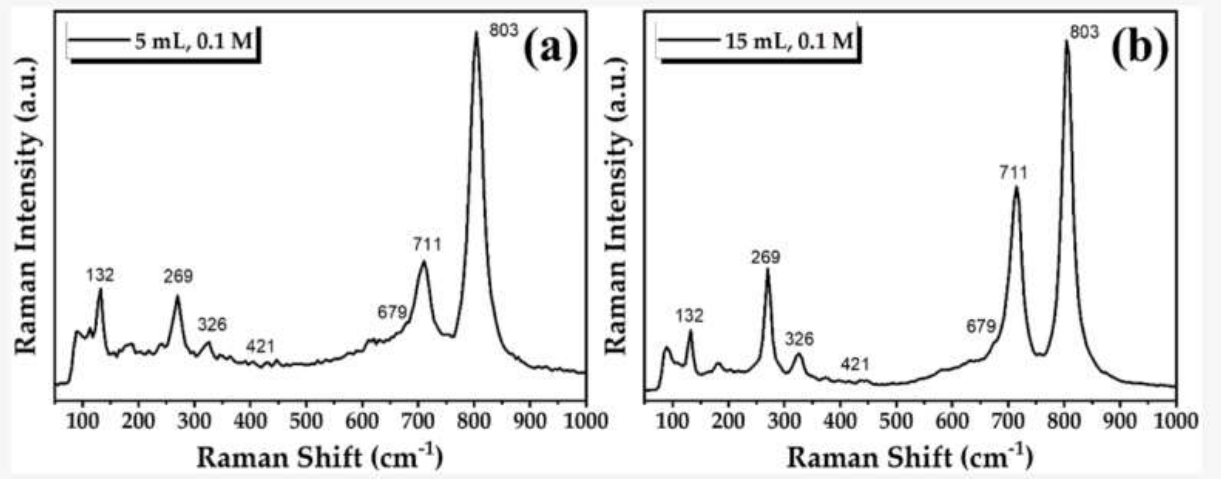

Fig. 2 Typical raman spectra of WO_3 thin films studied in this work [27].

Tin oxide films doped with aluminium were created using Ultrasonic Spray Pyrolysis. The Morphology of Tin Oxide films' morphology changed because of alpha doping, producing films with smaller grains. After Al doping, SnO_2 films experience a structural reordering and a textural transition from (301) to (101), and finally to (002) preferred Crystallographic Orientation. With Al doping, the lattice parameters (a and c) drop. With an average transmittance value of 72%-18%, Optical Transmission remains constant in the visible area.

On the other hand, when the Aluminium (Al) concentration in the grown films increases, the plasmon frequency in the near-infrared region changes towards the infrared region. The conductivity of nominally undoped SnO_2 is around 1120 S/cm. The reason for this increased conductivity is thought to be the Cl^- ions that function as donor dopants in the $SnCl_4{\cdot}5(H_2O)$ precursor. Due to compensation for the formation of holes, the addition of Al to the SnO_2 lattice resulted in a reduction in the material's electrical conductivity. The SEM picture of a nominally undoped SnO_2 film makes it evident that the films are Polycrystalline and that there are extensive planar twin faults that span the grains.

Furthermore, many extended twin faults can be seen inside a single grain, indicating a high defect density. It is noteworthy that these twin boundaries are undesirable because they are thought to represent extra locations for electron scattering, which is bad for SnO_2's electrical characteristics. In SnO_2:Al-0.2 and 0.4 films, the density of planar defects dropped significantly with doping. Lamellar twins are absent from films with greater Al contents. The sample, namely SnO_2:Al-5.2, was placed on Si and examined using TEM without any post-annealing processing [28]. The observed diffraction rings correlate well with SnO_2 indices. Regarding Al_2O_3, no one diffraction ring matches the Crystalline Alpha Phase or any other Polymorphs of Alumina. Al_2O_3 is present in extremely small amounts in the compositions under study. Consequently, there can be some Al_2O_3 spots in the diffraction pictures, but it is also probable that they exist.

Using an automated Nebuliser Spray Pyrolysis approach, Zinc-Doped Tin Oxide films were effectively created [29]. The super-linear resistance behavior is seen on the IV characteristic graph. A dynamic technique was used to study the Gas-Detecting behavior of the films, and the results show that a 1% Zn-doped porous SnO_2/SnO_2 thin film sensor was very sensitive to CO gas. As a result, it is likely that the manufactured Zn-doped porous SnO_2/SnO_2 thin film, which was created with 1% Zn doping, would work well as a CO gas sensor. There is nearly no fluctuation in either long-term or short-term stability, which suggests outstanding repeatability and excellent short-term stability.

On the other hand, it was reported that the sensor's initial reaction was unchanged primarily throughout 56 days of continuous testing, indicating that 1% of the Zn-doped porous SnO_2 bilayer showed high-quality properties. The sensor's response value was steady at 99.92% during the process, demonstrating the device's high reusability and robustness. The Zn: SnO_2/SnO_2 porous bilayer film in FESEM experiments has flake-like nanopores all over its surface. In the porous films, agglomerations of flat, spherically shaped nanoparticles were seen. The number of nano porosities decreases due to the presence of bigger nanoparticles. A decline in micro porosities might have an impact on Hydrophilicity. The film composition in EDX analyses (Figure 3) verifies that several elements, such as tin, zinc, and Oxygen, are present in the matching samples that have been created. The use of a glass substrate is what causes the presence of silicon.

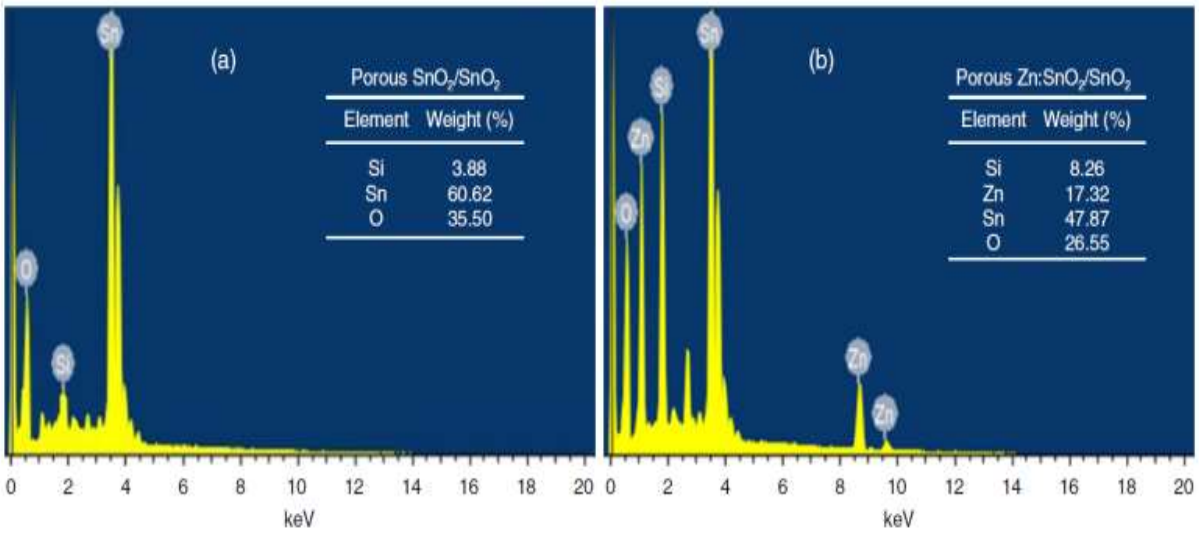

Fig. 3 EDX Studies of (a) SnO_2/SnO_2 Thin Films, and (b) Zn: SnO_2/SnO_2 Thin Film [29].

One excellent illustration of a p-type semiconductor is Nickel Oxide. This chemical has a stable broadband gap. When applied to p-type organic material, the dye absorbs light and then transfers electrons to the electrolyte and holes to the NiO thin film. When combined with Tungsten Oxide Films, Nickel Oxide Films exhibit Anodic Electrochromism and provide excellent device operating materials. To inject holes into Organic Light-Emitting Diodes, Nickel Oxide has a greater work function than Indium Tin Oxide. Thin coatings of Nickel Oxide were formed using Chemical Spray Pyrolysis. It was discovered that at 350 °C for the substrate temperature and 0.3 M for the precursor concentration, pure NiO thin films crystallized in the cubic phase [30]. After three hours of vacuum-annealed Nickel Oxide Thin Film annealing at 425 °C, it was found that the annealed samples outperform the films as-deposited. Weak diffraction peaks from the lattice planes (111) and (200) are seen in the diffraction pattern of the as-deposited thin film in XRD experiments (Figure 4(a)). On the other hand, as can be seen in Figure 4(b), the annealed NiO thin film had a brown hue, and the XRD pattern had firm peaks that matched the (111) and (200) orientations of cubic NiO.

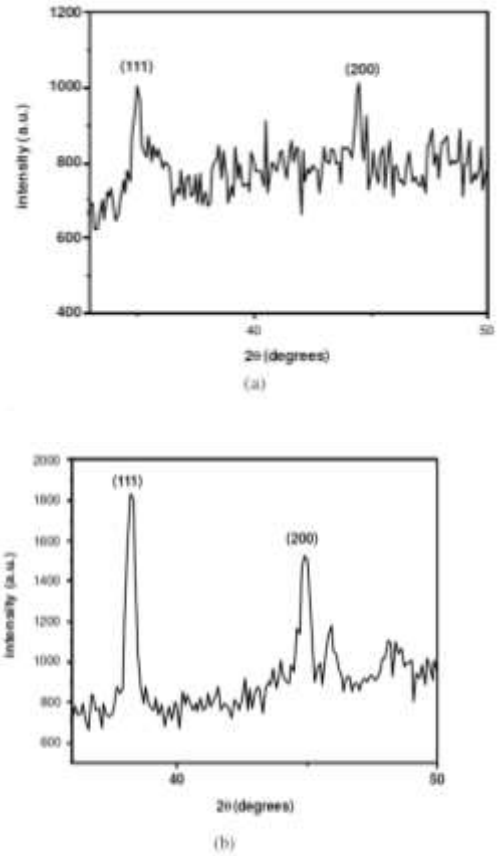

Fig. 4 XRD studies of (a) as-deposited, and (b) Annealed NiO films [30].

There have been encouraging suggestions for using copper oxide (CuO) thin films in chemical sensing applications. It has been specifically advised to use it as a sensitive layer for tracking dangerous and flammable gases. Its multitude of benefits, low cost, nontoxicity, and ease of manufacture make it an appealing material. Pure compounds could be confirmed through XRD [31] and Raman investigations (Figure 5). Additionally, peaks in the XPS analysis suggest the existence of Oxygen and copper. In contrast, these films' sheet resistance rises as the substrate deposition temperature rises, but the band gap reduces as the substrate deposition temperature increases.

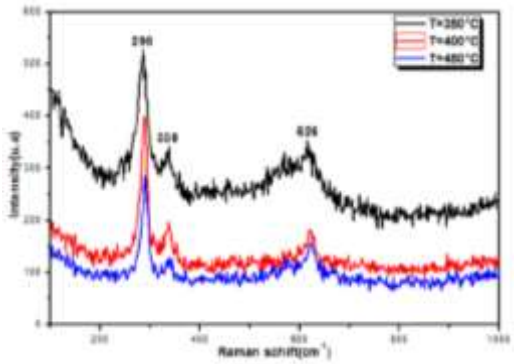

Fig. 5 Raman spectra of CuO films produced under different temperatures [31].

A lot of interest has been shown in Molybdenum Trioxide (MoO_3) due to its unusual, layered structure. With its strong optical transmittance and electrical conductivity in the visible spectrum, as well as its High Refractive Index and Relative Chemical Stability, it emerged as a notable progressive material. MoO_3 is a transition Metal Oxide semiconductor with three distinct crystal forms and a broad band gap (2.39-3.0 eV). The physical and chemical characteristics of these three phases are different. MoO_3 is used in solid catalysts, waveguides, gas sensors, batteries, pseudocapacitors, solar cells, and biological research. The Orthorhombic Phase of MoO_3 (α-MoO_3) was proven to be present in the films produced by the XRD peaks [32]. Images obtained with a FESEM showed their nanorod-structured shape. When the concentration of MoO_3 increases, the size of the micro-rods (4-0.8 μm) rapidly decreases. The length of the microrods that were seen can be used to infer this. The smooth surface of the microrods is evenly distributed and free of any holes or fissures. The pictures show an obviously damaged surface with formations that resemble randomly orientated islands. The existence of elements like Oxygen and Molybdenum is verified by EDX spectra. According to reports, the photoluminescence (PL) intensity of α-MoO_3 rods decreases in proportion to the pace at which photogenerated electron-hole pairs recombine. The type of substrate being utilized affects both the PL band's placement and intensity.

Rabeel and colleagues [33] synthesized the zinc oxide thin films on specific substrates, namely glass substrates. Since Zinc Oxide (ZnO) is Hydrophilic by nature, samples

deposited at ambient temperature exhibited this property, but films formed at 250 °C revealed this property to be Hydrophobic. Samples placed on heated substrates exhibited a greater degree of Crystallinity, according to the XRD data. Surface energy is reduced because of this improved Crystallinity. Furthermore, ZnO films improved surface coverage and roughness when using a 2 mL solution. Nonetheless, samples deposited at 30 mL demonstrated a consistent particle size distribution from 30-40 nm by taking advantage of the spray's distance from the sample to manage surface coverage and size distribution. It was observed that the samples with the highest level of roughness are those that are deposited 20 cm from the substrate. Thus, it can be shown that high roughness films are produced by increasing solution volume and lowering solution deposition distance. The bandgap rises in UV-visible Spectroscopy investigations when the substrates are heated to 250 °C. Less solution is deposited when the solution is sprayed farther from the substrate. The samples produced have a bandgap between 3.21 and 3.5 eV. According to the spectra, ZnO films are fully transparent in the visible spectrum but quite active in the ultraviolet.

Because of the electro-, photo-, and gasochromic characteristics of MoO_3 film, there has been a lot of interest in the material, leading to the creation of bright windows, display devices, sensors, lubricants, and optical switching coatings. Because these films are non-toxic, they may also be employed as antimicrobials. The nanocomposites [34] consist of a blend of water-soluble PEO polymer, chemically inert PVDF-HFP polymer, and antibacterial MoO_3 particles in a variety of sizes and morphologies. Because of their large specific surface area, MoO_3 nanowires dissolve rapidly in water (1 mg/ml) and at lower pH below 3.6 in under 3 minutes. The synthesis of films onto glass substrate under various concentrations has been emphasized by Supriya and colleagues [35]. These films are designated M1, M2, and M3, respectively. The films made with Molybdenum Oxide exhibited inhibitory action against P. aeruginosa for a period of up to 96 hours, and this activity changed as the concentration changed.

The inhibitory effect of thin films may vary in concentration and intensify as the concentration of the MoO_3 solution increases. Time-dependent antibacterial activity between test Pseudomonas and MoO_3 thin films was reported to peak at 6 hours of contact. Since the Antibacterial activity was not very substantial at higher concentrations, it was not considered. As the concentration of MoO_3 decreased, the inhibitory impact intensified. Additionally, the coating effectively lowers the number of viable cells in as little as six hours of contact time. Apart from the coating's inhibitory action, drying is another element that might impact the survival of cells on a glass surface. The coated surface dries up as exposure duration increases, and bacterial cells have less access to water, creating additional stress conditions that are necessary for cell survival. A possible explanation for the morphological structure of nano crystals is their antibacterial action. As the temperature rose, the ideal rod-shaped nano crystals developed and became effective against bacteria. Both spherical and nanorod-shaped structures were seen in FESEM tests (Figure 6). It was noticed that a larger rod width was found in the M3 sample (93.38 nm) compared to the M2 sample (56.3 nm). The film coating covered the whole surface of the glass substrate, notwithstanding the variations in the geometry of the granular formations.

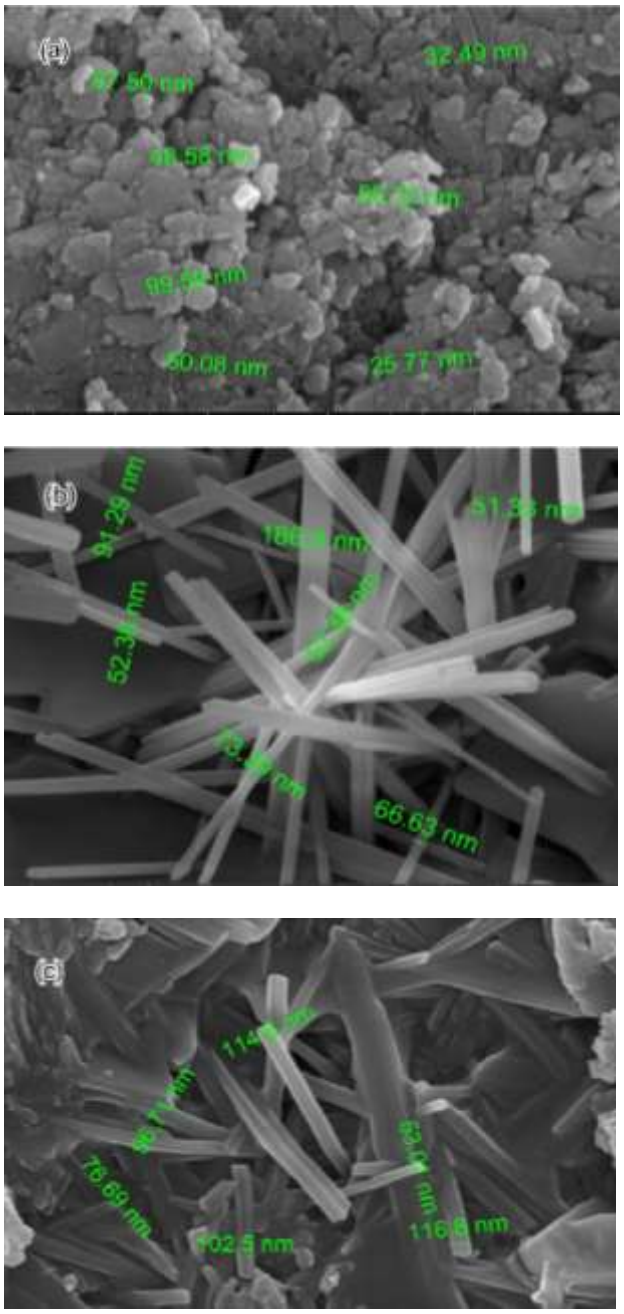

Fig. 6 FESEM studies for (a) M1, (b) M2, and (c) M3 [35].

In XRD studies, there are four diffraction reflections that could be found in pure nickel oxide films. However, diffraction peaks were shifted to higher angles in doped compounds. As a result, broader peaks could be observed in the Copper-Doped Nickel Oxide samples. In addition, larger sizes could be identified in the doped sample, representing Cu-Cu ion interactions that occurred. In Raman investigations, there are two significant peaks that could be observed at 550 and 1090 cm-1, indicating the formation of doped compounds. There was a slight change in the 2LO mode that could have been brought on by a larger Crystallite. In terms of gas sensing properties, p-type 4% Copper-Doped Nickel Oxide showed low resistance properties. The sensor element responds in 28 seconds and recovers in 21 seconds. HRTEM images of these films with Nanostructured Range (Figure 7), and Crystallinity that match the XRD pattern. The Polycrystalline character of the deposited film is confirmed by the SAED pattern.

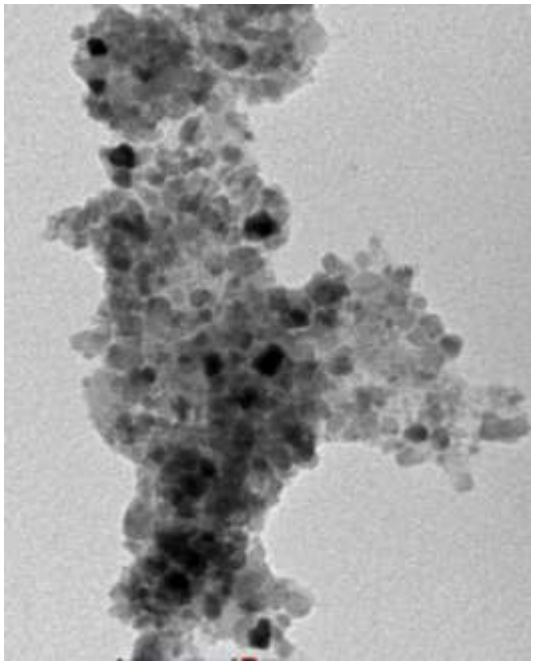

Fig. 7 TEM image of 4% NiO films [36]

Because oxide-based nanomaterials have far better stabilities than traditional organic dyes, they have drawn a lot of attention recently for application in bioimaging. Modified Flame Spray Pyrolysis (FSP) was proposed by Sovann and colleagues [37] as a scalable process to generate Tb-doped Y_2O_3, a Green Light-Emitting Phosphor, in the Nanometre size range. During the experiment, it was discovered that an Alkali Salt ($NaNO_3$), when combined with other Metal Nitrate Precursors, is a highly efficient size-controlling agent. The mixed solution underwent Flame Spray Pyrolysis, yielding oxide composites consisting of Y_2O_3:Tb^{3+} and Na_xO. Nevertheless, a simple water wash eliminated the salt byproduct. The Y_2O_3:Tb^{3+} nanoparticles generated by this salt-assisted FSP were well-dispersed and nano-sized, and their Luminescence and Crystallinity were greater.

The surface of the nanoparticles was functionalized with amino groups to facilitate the adhesion of biological molecules. Conversely, the study focused on the gas compositions at various flame settings. The flow rates of O_2 and CH_4 were adjusted to optimize the flame. The flame was longer and had a greater CH_4 flow rate; conversely, the flame got shorter when there was an O_2 gas supply. The highest temperatures of the flame fell at a 6 L/min CH_4 flow rate while the O_2 flow rate increased to 850, 775, and 700 °C. Nevertheless, when the CH_4 flow rate was raised to 9 L/min, the O_2 flow rate rose, as well as the flame temperature. Prior to being cleaned with water, the particles in TEM studies seemed to be coated in amorphous phases, which might be related to leftover sodium species. However, after washing with water, all the amorphous species disappeared. In TEM studies, a cubic phase with (222) plane was observed. The great Crystallinity of the particles is shown by the Selected Area Electron Diffraction (SAED) picture (Figure 8), whose dotted patterns show the cubic phase Y_2O_3's lattice planes (211), (222), (332), and (440).

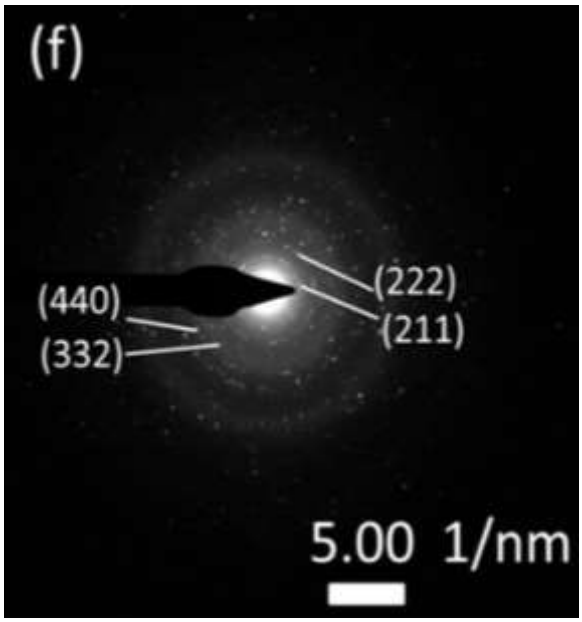

Fig. 8 Selected area electron diffraction of flame spray pyrolysis product [37].

5. Conclusions

Spray Pyrolysis has many advantages compared to other deposition methods. In the future, this deposition method will be chosen to prepare different types of thin film materials. Experimental results confirm that the prepared samples strongly depend on experimental conditions. Pure samples could be identified through XRD, Raman, and XPS techniques. Grain size could be studied via atomic force microscopy, scanning electron microscopy, and transmission electron microscopy. The prepared films could be used in different applications such as photovoltaics, sensor devices, laser devices, solar window coating, and optical imaging.

Funding Statement

The author was financially supported by INTI International University, Malaysia.

Acknowledgments

This research work was financially supported by INTI International University.

References

[1] Ghazi Aman Nowsherwan et al., "Numerical Optimization and Performance Evaluation of ZnPC:PC70BM based Dye-Sensitized Solar Cell," *Scientific Reports*, vol. 13, no. 1, pp. 1-16, 2023. [CrossRef] [Google Scholar] [Publisher Link]

[2] Ho Soonmin, and A.G. Jacob, "A Brief Overview of X-Ray Photoelectron Spectroscopy Characterization of Thin Films," *Research Journal of Chemistry and Environment*, vol. 28, pp. 142-160, 2024. [Google Scholar]

[3] S.R. Gadakh et al., "Effect of Complexing Agent on the Properties of Spray-Deposited Bi_2S_3 Thin Films," *Materials Chemistry and Physics*, vol 56, no. 1, pp. 79-83, 1998. [CrossRef] [Google Scholar] [Publisher Link]

[4] S.L. Jenish et al., "Improved Photo Sensing Properties of CuO Thin Films by Doping Fe using Nebulizer Spray Pyrolysis Method," *Journal of Photochemistry and Photobiology A: Chemistry*, vol. 462, 2025. [CrossRef] [Google Scholar] [Publisher Link]

[5] R.R. Chamberlin, and J.S. Skarman, "Chemical Spray Deposition Process for Inorganic Films," *Journal of the Electrochemical Society*, vol. 113, no. 1, 1996. [CrossRef] [Google Scholar] [Publisher Link]

[6] C.H. Lee, and L.Y. Lin, "Characteristic of Spray Pyrolytic ZnO Thin Films," *Applied Surface Science*, vol. 92, pp. 163-166, 1996. [CrossRef] [Google Scholar] [Publisher Link]

[7] Pramod Shankarrao Patil et al., "Characterization of Ultrasonic Spray Pyrolysed Ruthenium Oxide Thin Films," *Thin Solid Films*, vol. 310, no. 1-2, pp. 57-62, 1997. [CrossRef] [Google Scholar] [Publisher Link]

[8] J.C. Manifacier, "Thin Metallic Oxides as Transparent Conductors," *Thin Solid Films*, vol. 90, no. 3, pp. 297-308, 1982. [CrossRef] [Google Scholar] [Publisher Link]

[9] D. Craigen et al., "Spray Deposition and Properties of Electrochromic Tungsten Oxide Films," *Journal of the Electrochemical Society*, vol. 133, no. 7, 1986. [CrossRef] [Google Scholar] [Publisher Link]

[10] J.P. Mangalhara, R. Thangaraj, and O.P. Agnihotri, "Photoelectrochemical Conversion using Sprayed CdSe," *Bulletin of Materials Science*, vol. 10, no. 4, pp. 333-340, 1988. [CrossRef] [Google Scholar] [Publisher Link]

[11] Anju Thomas, and Kalainathan Sivaperuman, "Chemical Spray Pyrolysis Deposited ZnO/ZIF-8 and Cobalt Doped ZnO/ZIF-8 Composite Thin Films for Highly Sensitive and Selective Ammonia Sensing at Room Temperature," *Surfaces and Interfaces*, vol. 54, 2024. [CrossRef] [Google Scholar] [Publisher Link]

[12] J.M. Grace, and Jan C.M. Marijnissen, "A Review of Liquid Atomization by Electrical Means," *Journal of Aerosol Science*, vol. 25, no. 6, pp. 1005-1019, 1994. [CrossRef] [Google Scholar] [Publisher Link]

[13] Vinay Kumar Singh, "Thin Film Deposition by Spray Pyrolysis Techniques," *Journal of Emerging Technologies and Innovative Research*, vol. 4, no. 11, pp. 910-918, 2017. [Google Scholar] [Publisher Link]

[14] Hilal Kübra Sağlam et al., "Exploring the Influence of Zn Impurities on the Structural, Optical, and H_2 Sensor Properties of Ultrasonic Spray Pyrolysis-Grown MgO Thin Films," *Optik*, vol. 315, 2024. [CrossRef] [Google Scholar] [Publisher Link]

[15] Georg Hass, Maurice H. Francombe, and John L. Vossen, *Physics of Thin Films*, vol. 9, 1st ed., Academic Press, New York, 2013. [Google Scholar] [Publisher Link]

[16] Udit Kumar et al., "SILAR Deposited Antiviral Silver-Doped Ceria Nano-Films," *Surfaces and Interfaces*, vol. 51, 2024. [CrossRef] [Google Scholar] [Publisher Link]

[17] C.J. Nkamuo et al., "Tuning the Properties of Manganese-Doped Zinc Oxide Nanostructured Thin Films Deposited by SILAR Approach," *Chemistry of Inorganic Materials*, vol. 2, pp. 1-9, 2024. [CrossRef] [Google Scholar] [Publisher Link]

[18] C.R. Jácome-Martínez et al., "CuO Thin Films Deposited by the Dip-Coating Method as Acetone Vapor Sensors: Effect of their Thickness and Precursor Solution Molarity," *Micro and Nanostructure*, vol. 187, 2024. [CrossRef] [Google Scholar] [Publisher Link]

[19] Carlos E. Caballero-Güereca et al., "Transparent ZnO Thin Films Deposited by Dip-Coating Technique: Analyses of their Hydrophobic Properties," *Surfaces and Interfaces*, vol. 37, 2023. [CrossRef] [Google Scholar] [Publisher Link]

[20] Lazhari-Ayoub Naas et al., "Effect of TiN Thin Films Deposited by Oblique Angle Sputter Deposition on Sol-Gel Coated TiO_2 Layers for Photocatalytic Applications," *Thin Solid Films*, vol. 793, 2024. [CrossRef] [Google Scholar] [Publisher Link]

[21] A. Fernández García et al., "Femtosecond Laser Thinning for Resistivity Control of Tungsten Ditelluride Thin-Films Synthesized from Sol-Gel Deposited Tungsten Oxide," *Surfaces and Interfaces*, vol. 44, pp. 1-8, 2024. [CrossRef] [Google Scholar] [Publisher Link]

[22] Sefali R. Patel et al., "Thorough Investigation of the Optical, Electrical and Thermal Properties of Cu_3Se_2 Thin Film Deposited by Chemical Bath Deposition," *Thin Solid Films*, vol. 791, 2024. [CrossRef] [Google Scholar] [Publisher Link]

[23] Farzana Yasmin et al., "A Comprehensive Study on Structural and Optical Properties of Zinc Selenide/Poly Ortho-Methoxyaniline Hybrid Thin Films Deposited by Chemical Bath Deposition and Plasma Polymerization Techniques," *Arabian Journal of Chemistry*, vol. 17, no. 7, pp. 1-9, 2024. [CrossRef] [Google Scholar] [Publisher Link]

[24] M.O. Egbuhuzor et al., "Electro-Deposited Nanocomposite Coatings and their Behaviours against Aqueous and High-Temperature Corrosion: A Review," *Hybrid Advances*, vol. 5, pp. 1-10, 2024. [CrossRef] [Google Scholar] [Publisher Link]

[25] Ayush Owhal et al., "Remarkable Tribo-Mechanical, Anticorrosion and Antibacterial Properties of ZnCu/GNPs Composite Coatings Prepared by Electro-Co-Deposition Technique," *Journal of Alloys and Metallurgical Systems*, vol. 6, pp. 1-10, 2024. [CrossRef] [Google Scholar] [Publisher Link]

[26] Mohamed Amine Dahamni et al., "Spray Pyrolysis Synthesis of Pure and Mg-Doped Manganese Oxide Thin Films," *Coatings*, vol. 11, no. 5, pp. 1-12, 2021. [CrossRef] [Google Scholar] [Publisher Link]

[27] Kyriakos Mouratis et al., "WO_3 Films Grown by Spray Pyrolysis for Smart Windows Applications," *Coatings*, vol. 12, no. 4, pp. 1-12, 2022. [CrossRef] [Google Scholar] [Publisher Link]

[28] Getnet Kacha Deyu et al., "SnO_2 Films Deposited by Ultrasonic Spray Pyrolysis: Influence of Al Incorporation on the Properties," *Molecules*, vol. 24, no. 15, pp. 1-16, 2019. [CrossRef] [Google Scholar] [Publisher Link]

[29] R. Yogasaraswathi, and J. Dheepa, "Effect of Zinc Doping and Porosity on Structural, Morphological and Gas Sensing Properties of Porous Zn:SnO_2 Bilayer Thin Film," *Asian Journal of Chemistry*, vol. 36, no. 7, pp. 1579-1586, 2024. [CrossRef] [Publisher Link]

[30] S. Morkoç Karadeniz et al., "Properties of NiO Thin Films Prepared by Chemical Spray Pyrolysis using $NiSO_4$ Precursor Solution," *Asian Journal of Chemistry*, vol. 24, no. 4, pp. 1765-1768, 2012. [Google Scholar] [Publisher Link]

[31] Maha Hinna et al., "Elaboration and Characterization of CuO Thin Films by Spray Pyrolysis Method for Gas Sensors Applications," *Proceedings*, vol. 14, no. 1, pp. 1-2, 2019. [CrossRef] [Google Scholar] [Publisher Link]

[32] G. Lavanya, and N. Sivanandan, "A Facile Synthesis for Studying the Effect of Molar Concentration on Structural, Morphological and Optical Behaviour of MoO_3 Thin Films using Jet Nebulizer Spray Pyrolysis Technique for n-MoO_3/p-Si Photodiode Application," *Asian Journal of Chemistry*, vol. 33, no. 12, pp. 2999-3005, 2021. [CrossRef] [Google Scholar] [Publisher Link]

[33] Muhammad Rabeel et al., "Controlling the Wettability of ZnO Thin Films by Spray Pyrolysis for Photocatalytic Applications," *Materials*, vol. 15, no. 9, pp. 1-13, 2022. [CrossRef] [Google Scholar] [Publisher Link]

[34] Urška Gradišar Centa et al., "Polymer Blend Containing MoO_3 Nanowires with Antibacterial Activity against Staphylococcus Epidermidis ATCC 12228," *Journal of Nanomaterials*, vol. 2020, pp. 1-11, 2020. [CrossRef] [Google Scholar] [Publisher Link]

[35] Supriya Shukla, Anuradha Jape, and Sharda Gadale, "Study of Concentration and Temperature Dependent Structural, Optical, Photocatalytic and Antimicrobial Activity of MoO3 Thin Films by Ultra Spray Pyrolysis," *Asian Journal of Chemistry*, vol. 34, no. 6, pp. 1419-1424, 2022. [CrossRef] [Publisher Link]

[36] K. Rajesh, Nagaraju Pothukanuri, and M.V. Ramana Reddy, "Synthesis and Characterization of Pure and Cu-doped NiO Thin Films for Detection of Ethanol," *Asian Journal of Chemistry*, vol. 35, no. 5, pp. 1250-1256, 2023. [CrossRef] [Publisher Link]

[37] Sovann Khan et al., "Control of Particle Size in Flame Spray Pyrolysis of Tb-doped Y_2O_3 for Bio-Imaging," *Materials*, vol. 13, no. 13, pp. 1-14, 2020. [CrossRef] [Google Scholar] [Publisher Link]